






Impacts of the Red Sea and Persian Gulf on the Northern Indian Ocean in Numerical Simulations

Edmo J. D. Campos^{1,*}, Arnold L. Gordon², Geogenes Cavalcante³, Björn Kjerfve⁴, Mohamed Abouleish⁵

¹ Universidade de São Paulo - Instituto Oceanográfico (Praça do Oceanográfico, 191 - Butantã - São Paulo - 05508-120 - SP - Brazil)

² Columbia University - Lamont-Doherty Earth Observatory (61 Rte 9W - Palisades - NY 10964 - USA)

³ Universidade Federal do Alagoas - Instituto de Ciências Atmosféricas (Av. Paulo Holanda, 19 - Cidade Universitária - Maceió - 57073678. - AL - Brazil)

⁴ University of South Carolina - School of the Earth, Ocean and the Environment (701 Sumter Street - EWS 617. Columbia - SC 29208 - USA)

⁵ American University of Sharjah - College of Arts and Sciences (Building 7 - Sharjah - United Arab Emirates)

* Corresponding author: edmo@usp.br

ABSTRACT

Warm saline water masses emanating from the Persian Gulf (PG) and the Red Sea (RS) spread across a large area of the northern Indian Ocean upper layers, affecting the thermocline stratification, the circulation, and the air-sea exchanges over the Arabian Sea (AS) and Bay of Bengal (BoB). To explore the significance of these waters, we use numerical simulations to investigate the impact of isolating (closing) the RS and PG. The results show that the differences between the model runs, with and without the RS and PG, have marked effects on the AS and BoB seasonal variability. As expected, the major differences are concentrated in the surface mixed layer and thermocline of the AS. However, differences are also found further east in the BoB, mainly during the boreal summer. Significant differences are present in the air-sea freshwater and heat fluxes calculated by the model. In addition to the seasonality, there are significant interannual variability, with possible correlation with the El Niño-Southern Oscillation. Results of the experiments suggest that the upwelling in the Sri Lanka Dome, in the southwestern Bay of Bengal, would have responded differently to the 2009-2010 El Niño-La Niña in the absence of PG and RS input.

Descriptors: Persian Gulf, Red Sea, Indian Ocean, Arabian Sea, Bay of Bengal.

INTRODUCTION

The Red Sea (RS) and the Persian Gulf (PG), also referred in the scientific literature as the Arabian Gulf, inject into the Indian Ocean via the Gulfs of Aden and Oman, respectively, the most saline waters found in the world oceans (Beal et al., 2000; Bower et al., 2000; Rochford, 1964). The volume transports from the two marginal seas are

relatively small: ~ 0.2 Sv of Persian Gulf Water (PGW) and ~ 0.4 to 0.8 Sv of Red Sea Overflow Water (RSOW) (Beal et al., 2000; Bower et al., 2000; Durgadoo et al., 2017; Johns et al., 2003). Nevertheless, due to their unique thermohaline characteristics, the PGW and the RSOW can be tracked from their sources over great distances. Their imprint is evident within the upper kilometer, over an extensive area of the northern Indian Ocean (Beal et al., 2000; Bower et al., 2005, 2000; Wyrтки et al., 1971; You and Tomczak, 1993). As described in the cited works, the RSOW enters the Gulf of Aden with temperature close to 22°C and

Submitted: 22-Mar-2022

Approved: 03-Nov-2022

Associate Editor: Cesar Rocha



© 2022 The authors. This is an open access article distributed under the terms of the Creative Commons license.

salinity near 39, resulting in a density anomaly σ_θ of about 27.25 kg m^{-3} . After undergoing intense transformation in the Gulf of Aden, due to mixing with local fresher water, the RSOW reaches the Arabian Sea (ArS) with salinity in the range 35.8–36.0 (Bower et al., 2005). While in the Gulf of Aden, the RS plume is found confined within the 400–800m, with σ_θ ranging from 27.0 to 27.50 kg m^{-3} . After leaving the Tadjura Rift, water in same density range is found at depths 600–800m. In the ArS, this water mass is advected to the south along the continental slope deepening progressively, reaching 1000–1100m near 30°S (Bower et al., 2005). The upper 300 meters is dominated by waters originated in the PG (Campos et al., 2020a; Ezam et al., 2017; Johns et al., 2003). These waters spread over a large area reaching into the Bay of Bengal (BoB) (Hormann et al., 2019; Murty et al., 1992; Vinayachandran et al., 2013).

The lower salinity Indonesian Throughflow (ITF) and BoB exports are the primary balance to the salty ArS water. The substantial terrestrial freshwater inflow in the BoB contrasts with the ArS where, in addition to the RSOW and PGW inflows, there is an excess evaporation of the order of -0.11 Sv. The net result from precipitation, evaporation and river runoff in the BoB is of +0.13 Sv (Gordon et al., 2016; Murty et al., 1992; Vinayachandran et al., 2015). This causes a difference in sea surface salinity (SSS) greater than 3, more than the "salty" Atlantic versus the "fresh" Pacific. The SSS between the ArS and BoB basins depends on the efficiency of the interchange of their waters: the salty ArS invades BoB within the thermocline as BoB exports low salinity surface layer, in an estuary-like setup (Hormann et al., 2019). The heat and freshwater budgets in the BoB have a marked seasonal variability, with a strong influence of the summer monsoon. The intrusion of the salty ArS waters into the upper thermocline may affect the near-surface stratification with impacts on the air-sea exchanges (Vinayachandran et al., 2013).

An important feature associated with this exchange of waters between the ArS and the BoB is the Sri Lanka Dome (SLD), an upwelling system that occurs east of Sri Lanka, in the region delimited by 83°E and 5°–10°N (Burns et al., 2017; Cullen and Shroyer, 2019; de Vos et al., 2014;

Vinayachandran et al., 2004). By pumping up cooler, nutrient rich waters, the SLD affects biological productivity and air-sea exchange. The SLD is highly variable both in space and time, coupled to the seasonal monsoon forcing. It typically initiates in early June and is strengthened by the southwest monsoon winds. Then, it slowly migrates towards the northwest and dissipates by the end of September (Burns et al., 2017; Cullen and Shroyer, 2019; de Vos et al., 2014; Vinayachandran et al., 2004). The SLD is correlated with both the Indian Ocean Dipole (IOD) and strong El-Niño–Southern Oscillation (ENSO) events (Burns et al., 2017; Cullen and Shroyer, 2019).

Despite its relatively small volume, the extreme saltiness of PGW is expected to have significant impact on the thermohaline stratification, circulation, and air-sea exchanges over the northern Indian Ocean, including the eastern realm of the BoB and the SLD. The Persian Gulf is an evaporative basin. The increased salinity due to global warming, associated with the effects of the increasing freshwater production in desalination plants in the region, will certainly magnify the impacts of that marginal sea (Campos et al., 2020b). Thus, improved knowledge of the PGW spatial and temporal spreading patterns and their impact on the Indian Ocean oceanography is crucial to better evaluate the impact of the climate change induced intensified hydrological cycle in the Indian Ocean. In a previous study, the effects of different forcing mechanisms on the Indian Ocean salinity distribution were investigated in a suite of numerical experiments with a 4½-layer model with a thermodynamically active mixed layer (Han and McCreary Jr., 2001). It was found that some of the Persian Gulf waters, originally injected in a deeper layer (layer 3) in the Gulf of Oman, eventually entrains into the surface mixed layer, increasing the surface salinity by 0.1–0.2 in the Arabian Sea. From the Red Sea, waters entering in layer 4 increase the salinity values in this layer throughout much of the Indian Ocean, but particularly in the Arabian Sea and the western regions of the basin.

To further address the question on the importance of the PGW and RSOW in the Indian Ocean, two numerical experiments are carried out. In the first one, hereinafter referred as the Control

experiment, it is considered a realistic representation of the Indian Ocean basin to the north of 30°S, including the Persian Gulf and the Red Sea. In the second (henceforth NoAGRS), the two marginal seas were completely masked out. Because of the more pronounced presence of the PG waters in the upper 300 meters, on a large area from the ArS to the BoB, and our interest on the air-sea interactions and near surface dynamics, we will focus the analysis on the impacts of closing the Persian/Arabian Gulf.

Our study is structured as follows. In Section Methods, the numerical model, its set-up, and the data used to validate the results are described. In the following section, the results of the numerical experiments are described and discussed. Finally, the final Section presents a summary and the Conclusions of the most relevant findings.

METHODS

THE NUMERICAL MODEL

The experiments were run with an implementation of the Hybrid Coordinate Ocean Model (HYCOM; <https://www.hycom.org>) (Bleck, 2002; Halliwell, 2004) to the geographic region delimited by latitudes 30°S–31°N and longitudes 30°E–115°E (Figure 1), with nominal horizontal resolution of 1/12 of a degree (in the N-S direction the grid spacing is multiplied by the cosine of latitude). The vertical stratification was represented by 22 hybrid layers, designed to have a higher resolution of the upper 1000 meters of the water column. All 22 layers were allowed to transform from isopycnic to terrain-following or to z-coordinates. The bathymetry was based on the NOAA-NGDC's ETOPO5 dataset (Smith and Sandwell, 1997). The shallowest depths were kept in 5 meters -- regions with depths less than 5 meters were considered land.

The one-way nesting approach to provide the initial and boundary conditions is described as follows. First, six-days averages of all relevant fields from a HYCOM global run (GLBa0.08) were remapped from 32 σ_2 layers to 22 isopycnic surfaces and interpolated to the horizontal grid defined for the two present experiments. The model was then forced

with NCEP 1 Reanalysis products (Kalnay et al., 1996); (<https://psl.noaa.gov/data/gridded/data.ncep.reanalysis.html>), namely: surface air temperature, net downward radiation flux, net downward shortwave flux, precipitation, vapor mixing ratio, surface wind speed and wind stress. The experiment extended from January 2000 to December 2013. At each time step, the products of the model's integration were relaxed to the boundary conditions, in a 36 grid-points lateral buffer zone, with an e-folding time of 53 days. Values at grid-points farther than 1.5 degrees from the lateral open boundaries would be retained. Otherwise, inside the 36-grid points nesting boundary layers, values would tend gradually towards those provided by GLBa.08 on the open boundaries.

Two experiments were run. In the first, the entire oceanic region from ETOPO5 was considered, including the Red Sea and the Persian Gulf. For the second, the bathymetry file was edited converting into land the PG and the RS (shown as the white area in Figure 1. Because the major interest was to investigate the role of the PGW and RSOW, no rivers were considered in the simulations but, in both cases, the sea surface salinity and sea surface temperature were relaxed to the WOA2018 climatology, with an e-folding time of 30 days. In this way, the model retains "memory" of the climatological freshwater distribution in the mixed layer. The output of the integration for both the internal (baroclinic) and external (barotropic) modes were saved for the entire grid at a one-per-day frequency. The size of the raw dataset containing all variables for the entire run is over one terabyte in binary (Fortran) format. The complete dataset can be downloaded via anonymous ftp, upon request. However, the minimum amount of the processed data necessary for reproducing the analyses reported in this paper, sized over 5 gigabytes in compressed NetCDF format, is freely available in an open access repository: <https://www.seanoe.org> (Campos, 2020).

DATA FOR MODEL VALIDATION

To evaluate the model's accuracy, the results were compared with gridded products of temperature, salinity and mixed layer depth provided by the

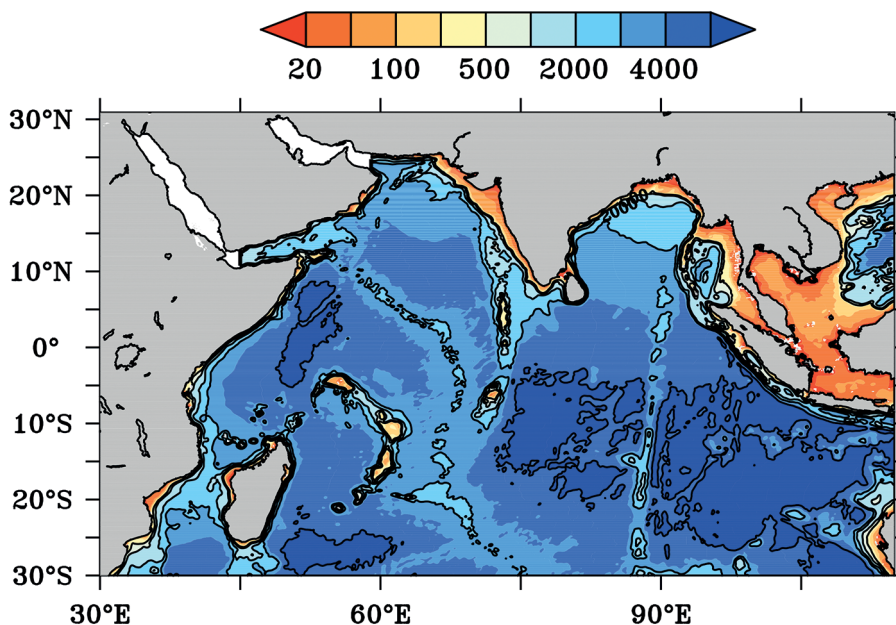


Figure 1. Bathymetry based on ETOPO5 (Smith and Sandwell, 1997) used in the experiment in which the Persian Gulf and the Red Sea were not considered (Experiment NoAGRS).

Argo Program available at <http://www.argo.ucsd.edu> (<http://doi.org/10.17882/42182>), for the period extending from January 2004 to December 2016.

In preparation for the use of this data set in the model's validation, seasonal (summer and winter) horizontal maps and vertical profiles of salinity in the upper four hundred meters of the northern Indian Ocean were plotted. As seen in Figure 2, in the uppermost 50m layer, the horizontal salinity distribution shows marked seasonal variation. In the January, February and March (JFM) season (**a**), fresher waters from the BoB are exported to the ArS along two main pathways, as described in a previous work based on Argo data, surface drifters and satellite data (Hormann et al., 2019). In the first one, located in the western region of the BoB, surface freshwater export during JFM is mainly associated with the westward flowing Northeast Monsoon Current (NMC), along the east coast of India and around Sri Lanka (Hormann et al., 2019; Schott et al., 2009). As described in the literature (Hormann et al., 2019), the freshwater exported from BoB does not appear to flow northwestward along the Indian west coast beyond approximately 10°N. As much as in the cited work, to the south of the NMC, between 5°S

and 5°N, the high salinity waters from the ArS are transported towards the eastern Equatorial Indian Ocean by the South Equatorial Counter Current (SECC). In the second pathway, waters from the BoB flow southward along the eastern boundaries of the BoB, cross the equator and then veer westward as part of the South Equatorial Current (SEC). In July-August-September (JAS), shown in Figure 2 (**b**), the surface-layer flow around Sri Lanka reverses direction, with the Southwest Monsoon Current (SMC) transporting ArS water into the BoB. The SECC is somewhat displaced southward and a tongue of lower salinity water protruding into the ArS appears between the SMC and the SECC.

Within the layer defined by depths 100m and 150m, export of BoB waters into the ArS is considerably reduced in both seasons, with basically a year-round export of saltier ArS waters into the BoB. The seasonality is in the apparent intensity of the flow and in the northernmost latitudes reached by the ArS waters. Both during JFM and JAS (Figure 2 **c,d**), saltier waters flow around Sri Lanka towards the BoB. In JAS, however, these waters reach much further north along the eastern coast of India. Below 200m (Figure 2 **e,f**), the

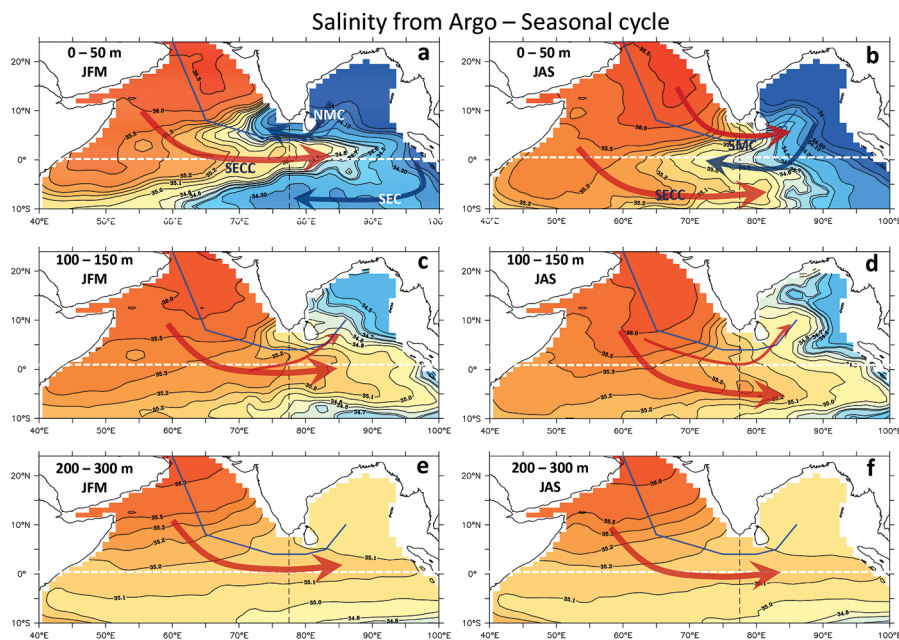


Figure 2. Horizontal distribution of salinity, from Argo, averaged over 0-50m (top), 50-150m (mid) and 200-300m (bottom) for JFM (left) and JAS (right). The thin blue line from the Gulf of Oman to the BoB indicates where vertical profiles were plotted. The curved arrows indicate the main currents in the region related to the water interchange between the ArS and the BoB, according to (Schott et al., 2009).

seasonality practically vanishes, with the saltier waters spreading all over the BoB.

The upper 300 meters in the ArS is dominated by waters from the Persian Gulf (Bower et al., 2000, 2005; Campos et al., 2020a; Ezam et al., 2017; Johns et al., 2003). Thus, it is likely that most of the water being exported into the BoB, at all depths considered in Figure 2, are predominantly from the Gulf of Oman. To have a better view of the structure of the presumably Persian Gulf water mass, according to Argo data, vertical profiles of salinity along a line extending from the mouth of the Gulf of Oman (see Figure 2) to the BoB were plotted, as shown in Figure 3. The seasonality in the near-surface layer (0-50m) is evident in the top 150m during the winter (JFM). It is also clear from this vertical profile the intrusion of the saltier ArS waters into the BoB in the layer from 50m down to 150m. In the JFM season (upper panel), the salinity structure shows a well-defined estuary-like circulation. From the surface to approximately 50m depth, there is a layer of fresher BoB waters over a tongue of saltier waters protruding from the ArS into the BoB. Figure 3 also suggests that below 150m there is a secondary tongue of saltier waters into the BoB, in both seasons.

RESULTS & DISCUSSION

MODEL SPIN-UP AND EXPERIMENT'S TIME-HISTORY

Both experiments were started on 1-Jan-2000 and let to run until Nov-27-2013. The time-history of each realization is represented by the time series of the basin-averaged sea surface height (SSH) and kinetic-energy (KE), plotted in Figure 4. The upper panel (a) shows that it takes about four to five years for the model to reach a state of reasonable equilibrium in both experiments. The plots show that the differences in the mean surface elevation (b) and mean kinetic energy (c) between the two experiments are small. However, they are not completely negligible, especially for the kinetic energy (KE). They present interesting seasonal and interannual variability. In some periods the difference in KE reaches up to 10% of the corresponding values in the Control experiment. The seasonal variation is certainly linked to the Indian Ocean monsoon system. The interannual periodicity seems to be of a couple of years. As highlighted by the two vertical dashed lines in Figure 4, relatively large differences occurred

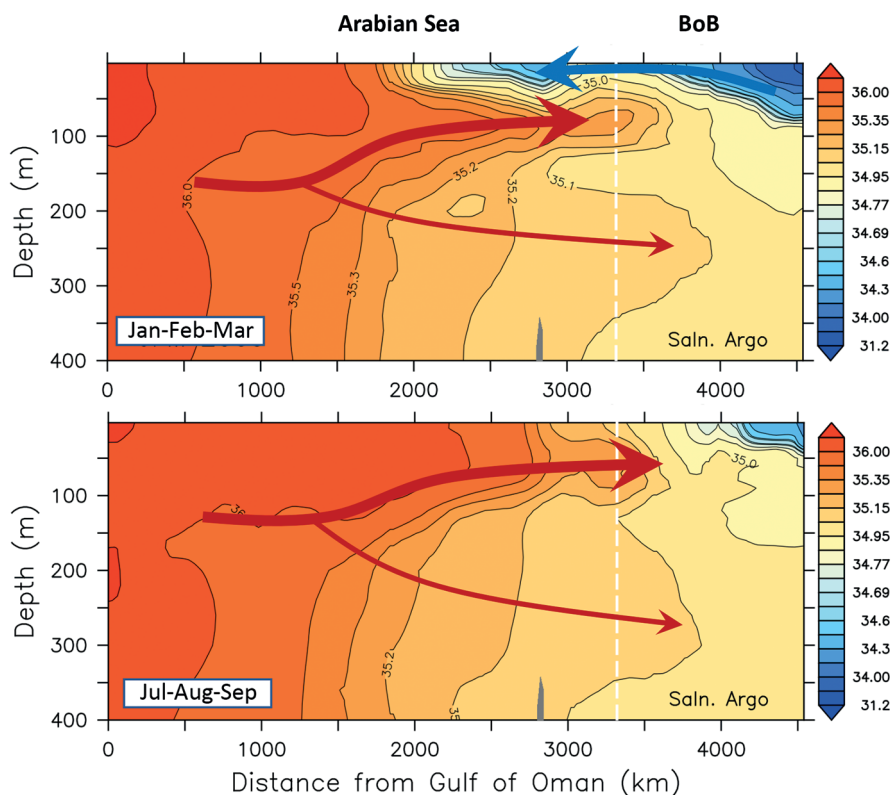


Figure 3. Vertical profiles of salinity, from Argo, along a line from the Gulf of Oman to the BoB, as indicated in Figure 2.

during 2009–2010, a period that, incidentally, coincides with the occurrence of an intriguing El Niño–La Niña sequence. Thus, the analyses in the following sections of the manuscript will emphasize the 2009–2010 period.

MODEL VALIDATION

To proceed with a more detailed investigation on the effects of closing the RS and PG, an evaluation of the model's results is made by means of a comparison with previous studies and with salinity and temperature data sampled with Argo floats. It is found that the model reproduces quite well the overall patterns of the seasonal wind-driven circulation (Figure 5) in the upper layers, in good agreement with the general patterns described in the literature (Hormann et al., 2019; Schott et al., 2009). It does also a good job in reproducing the seasonality in the exchange of waters between the ArS and the BoB. This is clear in the model's horizontal salinity distribution in the mixed layer (the color

shadings in Figure 5), which compares quite well with the Argo data in the upper layers (see Figure 2). For both Argo dataset and model, the salinity distribution follows the climatological circulation pattern. During JFM, in the region around southern India and Sri Lanka, to the north of the Equator, the surface circulation is dominated by a zonal current system oriented predominantly towards the west (the NMC), advecting fresher BoB waters into the ArS. In the summer (JAS), the mean salinity distribution also reflects the reversion of the currents, with an eastward flow (the SMC) advecting saltier waters into the BoB. In Figure 5, the 34.8 isohaline (red curve) highlights the frontier between regions of higher and lower salinity.

The accuracy of the model's results is further investigated by comparing the horizontal salinity distribution in both experiments with Argo data for the winter (JFM) and summer (JAS) of 2009. As seen in Figure 6, except for the differences in the salinity tongue advancing toward BoB, the model's

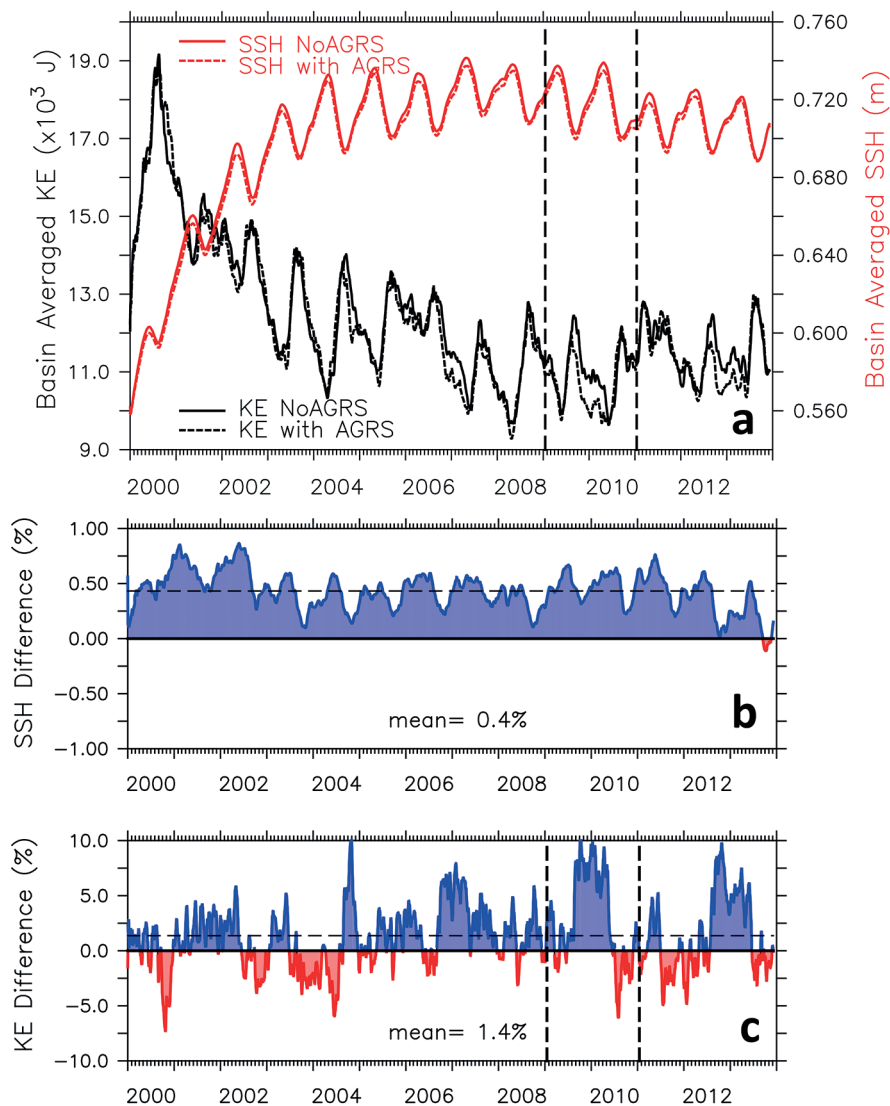


Figure 4. (a) Time-history of the basin averaged SSH and KE for both Control and NoAGRS experiments; (b) and (c) time series of the differences of SSH and KE in the two experiments. The dashed vertical lines indicate the 2009-2010 period, in which the KE difference reached values as high as 10% of the corresponding values in the Control experiment.

results for this particular year are also in good agreement with the data. The mixed layer salinity maps from the two experiments compare well with Argo data and are quite like each other. But, as it will be shown in the next Subsection (NoAGRS vs Control), some interesting differences can be noticed between the two runs, mostly in the Arabian Sea but, also in the vicinity of Sri Lanka and in the western part of the BoB. In JAS, for the NoAGRS case, the salinity tongue seems to extend a little

farther east than in the Control experiment. In this season, some significant differences are noticed within the SLD region and near the east coast of India in the BoB.

To complete the comparison with Argo data, TS-diagrams are plotted on some points along the line starting from the entrance of the Gulf of Oman to the Bay of Bengal, as indicated in the map in the upper-left panel of Figure 7. We will focus on the TS curves clustered in four different regions:

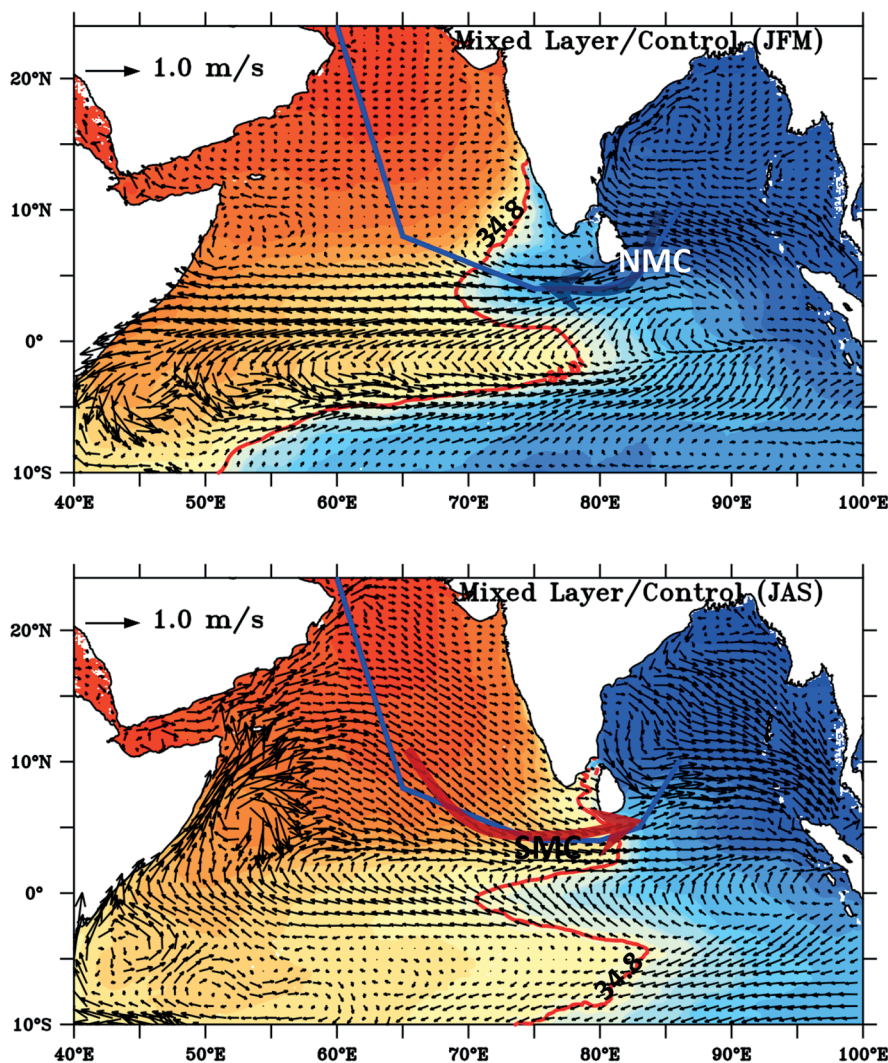


Figure 5. Color shading: seasonal winter (JFM) and summer (JAS) horizontal salinity distributions from the model's Control experiment (mixed layer). Vectors: the mixed layer seasonal velocity fields from the Control experiment. The averaging was done after removing the initial five years of the time series.

one in the northern (red color) and other (orange) in the southern part of the ArS, a third one (blue) around 4°–5°N, and the fourth (purple) in the SLD region. Although the thermohaline structure mostly agrees with the Argo data, the model fails to reproduce the subsurface salinity maximum, around $T=16^{\circ}\text{C}$, in the TS-diagrams from North Arabian Sea (red lines). Also, the intra-cluster variability is greater in the Argo data. This may affect the mean values and result in non-negligible differences between Argo data and model runs in Fig. 8. However, for the JAS-2009 season, as shown in Figure 7, as well as for JFM-2009 (not shown),

there is a good general agreement between the model's thermohaline structure with that sampled by the Argo floats. The vertical dashed lines indicate salinity 36.6 and 35, which roughly represent, respectively, the salinity values in the thermocline (the gray-shaded area in the TS-diagrams) near the Gulf of Oman and in the southern limits of the SLD.

NoAGRS *VERSUS* CONTROL

In the TS diagrams (Figure 7), there are small but noticeable differences between the experiment without the Arabian Seas (NoARS) and Control.

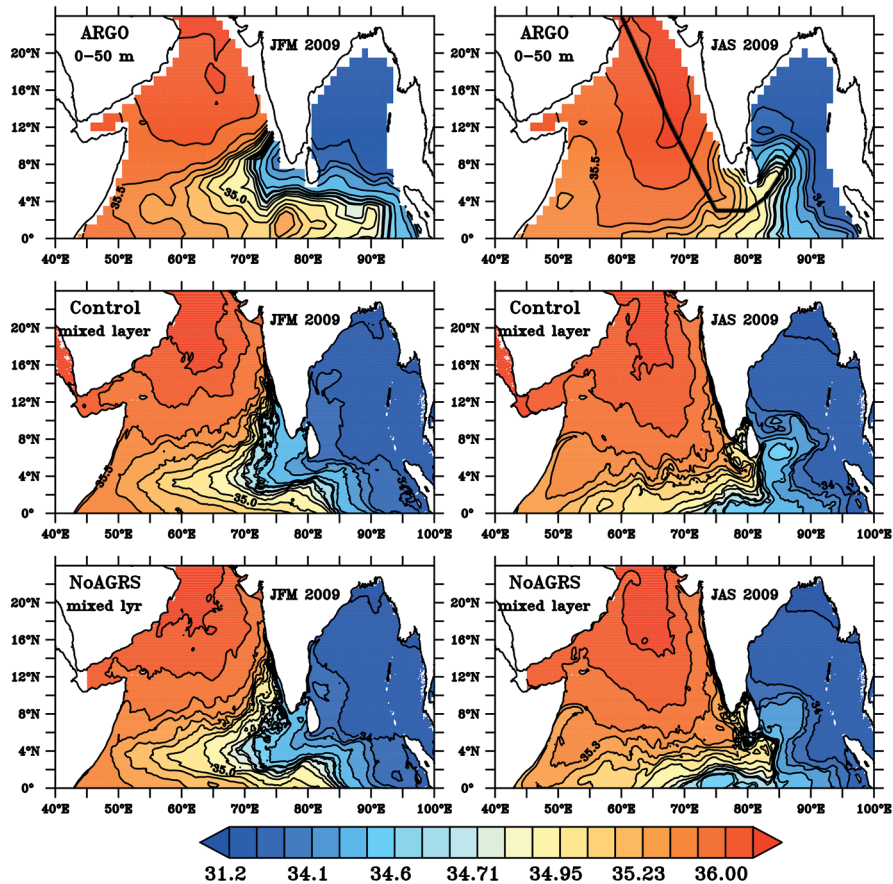


Figure 6. Horizontal distributions of salinity for JFM and JAS of 2009, for Argo (0-50m, top panel), Control (mixed layer, mid panel) and NoAGRS (mixed layer, bottom panel).

This is particularly true in the thermocline (shaded gray area in the TS-diagrams) and in the surface layers. To look further into the differences, TS-diagrams were plotted for temperature and salinity averaged over four of the six different segments along the line indicated in the map in Figure 7, for the JAS-2009 season. These are indicated in Figure 8 as the North and South Arabian Sea, the 4°–8° N band, and the SLD. The black curve is from Argo data and the red and blue from Control and NoAGRS, respectively. The largest differences occur near the Gulf of Oman at thermocline depths, as it should be expected, and in the upper thermocline and mixed layer in the SLD, what is not so obvious. According to these plots, in the absence of the Persian Gulf outflow, waters near the entrance of the Gulf of Oman, on a specific isopycnic surface at thermocline level, would be

less saline and consequently cooler. In The SLD region, the experiments suggest the opposite. On a specific density surface, in the NoAGRS case, waters would be saltier and warmer, an indicative that the SLD upwelling would be reduced during the JAS-2009 season.

As expected, because of the interruption of the Persian Gulf salty water inflow, which is normally present at thermocline levels in the Gulf of Oman (Campos et al., 2020a; Ezam et al., 2017; Johns et al., 2003), the closure of the PG results in a significant decrease in salinity between the isopycnals 25 and 28 $kg\ m^{-3}$ (the shaded area in Figure 7 and Figure 8). To better evaluate these differences, additional diagnostics are carried out starting with the horizontal distributions of salinity, temperature and velocity within the model's thermocline and the depth of mixed layer, as shown

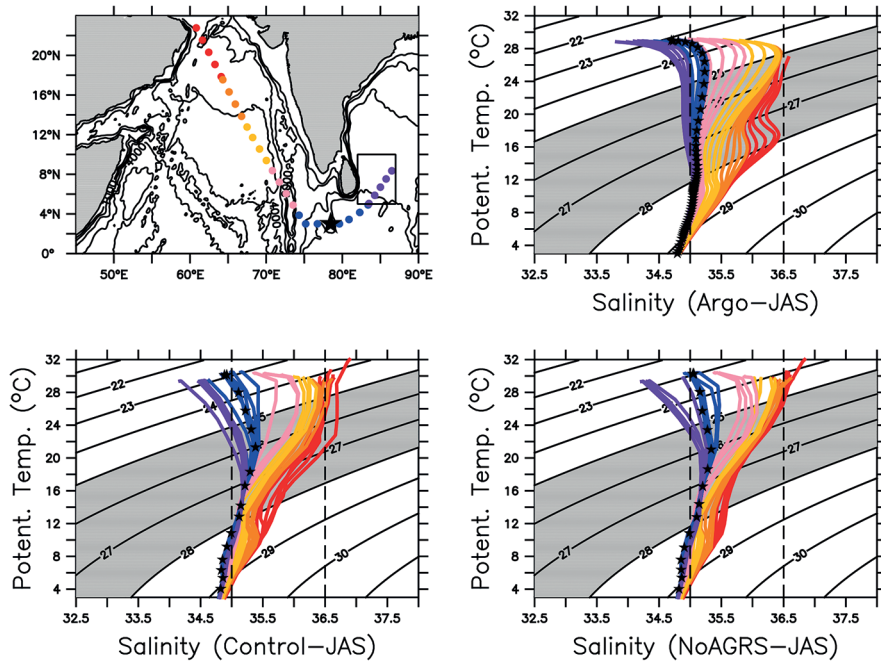


Figure 7. TS-diagrams from Argo and the two numerical experiments for JAS-2009, for T and S on the points indicated on the map in the upper left panel. The TS curve with black stars represents the T and S on 77.5°E, considered here as the longitude separating the ArS and the BoB.

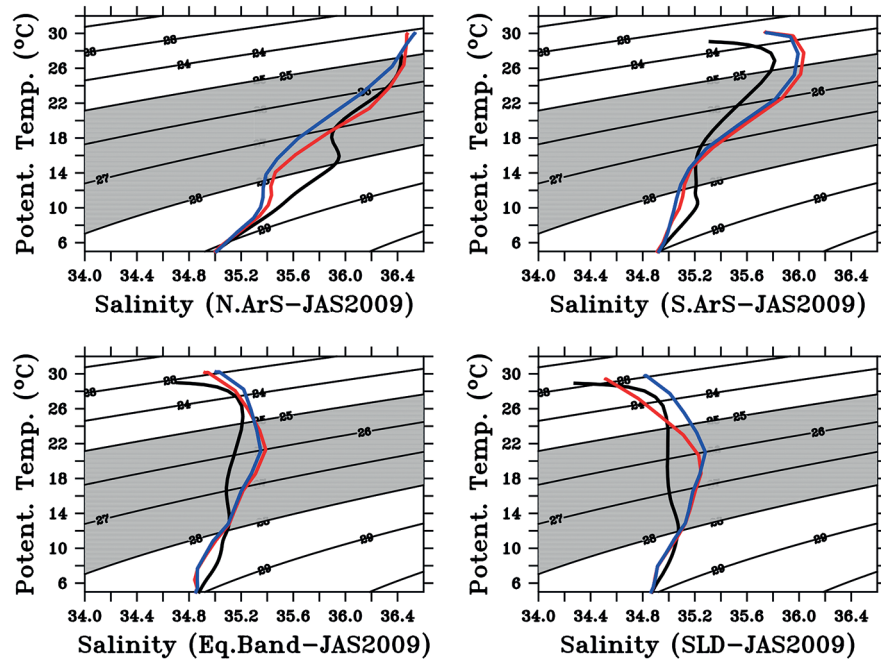


Figure 8. TS-diagrams with T & S averaged over four different segments of the line shown in the upper left corner of Figure 7: North and south Arabian Sea, equatorial band and SLD, for JAS-2009. The black curve is from Argo data. The red and blue are from Control and NoAGRS experiments, respectively.

in Figure 9 and Figure 10. In these two figures, the left panels (**a**, **c**, **e** and **g**) show the variables from the Control experiment with the differences (NoAGR minus Control) displayed on the right side (**b**, **d**, **f** and **h**). The temperature differences in the uppermost right panel (**b**) of Figure 9 and Figure 10 show that experiment NoAGRS has slightly higher temperatures in the zonal band 4°–8° N, around southern India and Sri Lanka, in both seasons (JFM and JAS). Despite the patchy distribution, it seems that NoAGRS in general has slightly lower temperatures in the ArS and higher in the BoB region. Similar distribution is seen for salinity in the upper-mid panel on the right (**d**), for both seasons. In general, salinity is higher in NoAGRS in the 4°–8° N band and in the BoB and lower in the ArS. For both seasons, the lower-mid panel (**f**) on the right show that there is an overall deepening

of the mixed layer, with a clear seasonal difference in the SLD. The changes in the mixed layer depth within the rectangle drawn east of Sri Lanka show intensified negative and positive values during JAS. These changes are also present in the thermocline salinity and temperature distribution within SLD, shown uppermost two left panels (**b** and **d**) in the JAS season.

The bottom-right panel (**h**) in Figure 9 and Figure 10 represents the differences in the velocity within the thermocline for JFM and JAS. In the two seasons, there are differences of up to 0.5 m s^{-1} , mainly near the western boundaries of the ArS. However, regions of higher differences are noted the northwest regions of the BoB in JFM. Within the SLD region, no noticeable differences are seen in JFM. While some differences are still present in the NW BoB during JAS, in this season

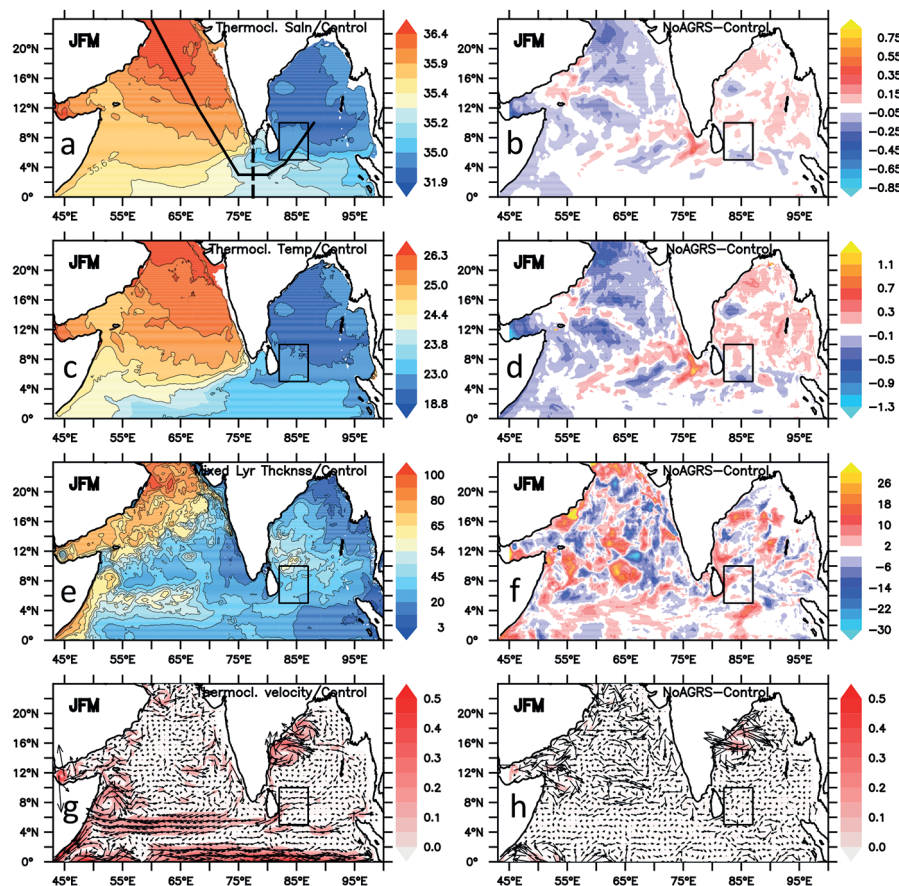


Figure 9. Horizontal distributions of salinity (**a**, **b**), temperature (**c**, **d**) and velocity in m s^{-1} (**g**, **h**) within the model's thermocline, and the depth in meters of the model's mixed layer (**e**, **f**) - JFM.

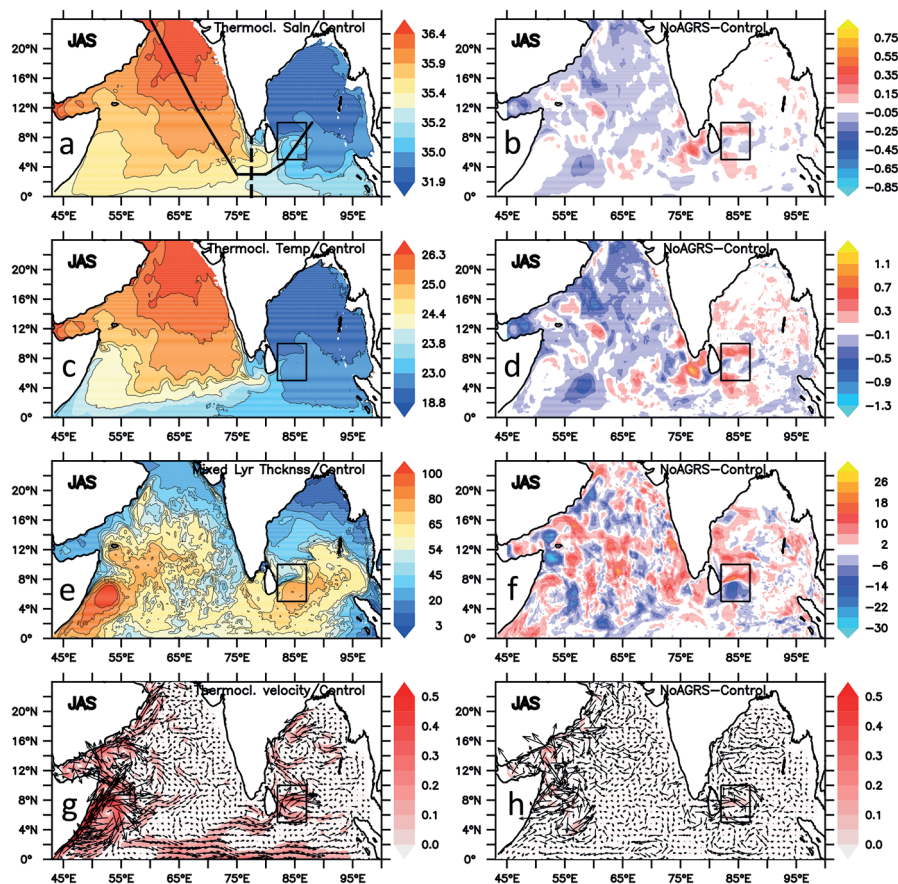


Figure 10. Horizontal distributions of salinity (a, b), temperature (c, d) and velocity in m s^{-1} (g, h) within the model's thermocline, and the depth in meters of the model's mixed layer (e, f) - JAS.

the largest differences are found within the SLD. In the summer (JAS), there is a pair of cyclonic and anti-cyclonic intensification which, as will be detailed below, agrees with the changes in the mixed layer depth, and in the thermocline's temperature and salinity, in the SLD region.

Because of its immediate connection to the PG and RS, the Arabian Sea is naturally more prone to be affected by the closure of the two marginal seas. However, the impacts on more remote regions such as the 4° – 8° N band and the Bay of Bengal are not so obvious. Thus, to better understand the changes displayed in Figure 9 and Figure 10, more detailed maps of the sea surface height (SSH) and mixed layer velocity were plotted for the region delimited by longitudes 77° E, and 95° E and the equator and latitude 20° N. In Figure 11, snapshots of the differences between values during JAS and the long-term mean in

Control are shown at approximately 15-days intervals, from 1-Jun-2009 to 1-Oct-2009. This difference was adopted to highlight the summertime anomalies in the two fields. In the first panel, on the upper left corner, a nucleus of cyclonic circulation can be seen within the rectangle defining the SLD region. The blue colors associated with the cyclonic eddy (the SLD) indicate a depression in SSH, what corresponds to an uplifting of the mixed layer depth (upwelling). Another region of intense upwelling is seen near the east coast of India, centered around 83° E, 15° N. The sequence of maps shows that the SLD traveled slowly northwestward, being gradually replaced within the rectangle by an anticyclonic eddy coming from southeast. In the higher latitudes, off east India, intense mesoscale variability is observed, with a succession of cyclonic and anticyclonic vortices.

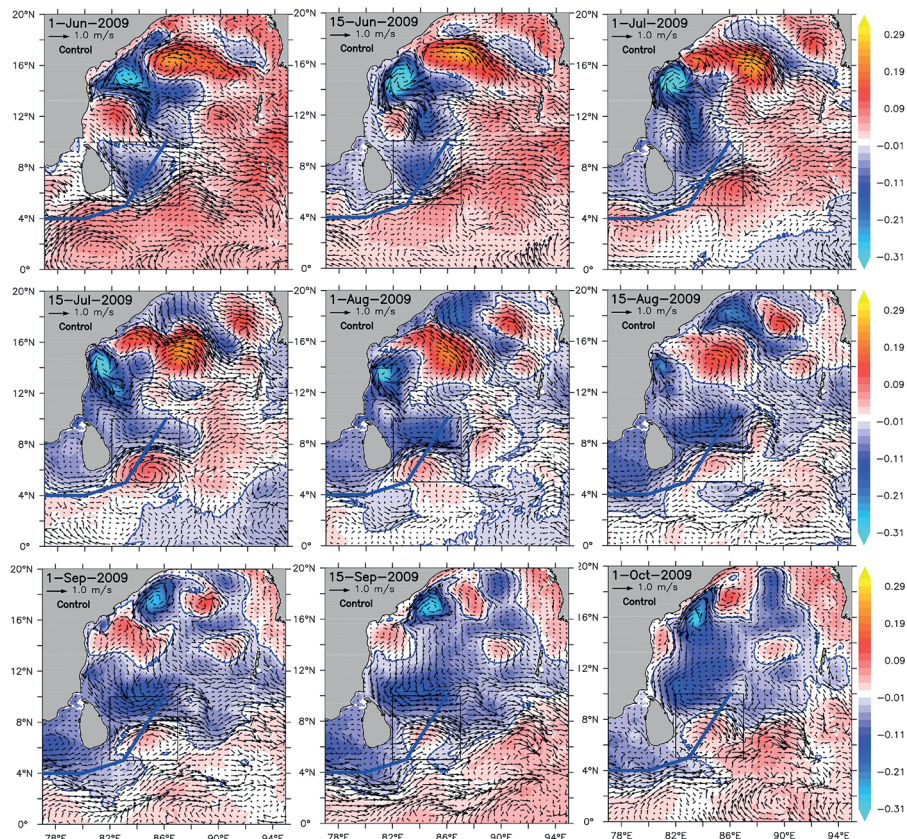


Figure 11. Snapshots of the differences in SSH and mixed layer velocity, between NoAGRS and Control, during JAS minus the long-term mean, at approximately 15-days intervals, from 1-Jun-2009 to 1-Oct-2009.

To evaluate the residual effect of the meso-scale variability, maps of the seasonal mean (June to Sep) of the SSH and mixed layer velocity in the Control experiment, and the mean difference (NoAGRS minus Control) were plotted, as shown in Figure 12. The result shows that the seasonal mean circulation within the rectangle off Sri Lank (left panel) is dominated by a pair of anticyclonic (in the south) and cyclonic (more to the north) vortices. More to north, the mean distribution shows a zonally oriented stripes of upwelling and downwelling region. The differences, displayed in the right panel of Figure 12, suggest that the closure of the PG and RS results in an overall tendency to counteract the cyclonic and anticyclonic centers, reducing the strength of both upwelling and downwelling processes.

For a clearer view of the impacts of NoAGRS in the water column, vertical profiles of temperature and salinity along the line from the Gulf of Oman

to the SLD region, for JFM and JAS in the two experiments, as well as the differences between the two cases were plotted and shown in Figure 13 and Figure 14. In these figures, the two solid white curves indicate the isopycnic surfaces $\sigma_{\theta}=23.25 \text{ kg m}^{-3}$ and $\sigma_{\theta}=25.77 \text{ kg m}^{-3}$, the 6th and 10th layers within the model's thermocline. The vertical dashed white line marks the longitude separating the ArS to the Bay of Bengal (as indicated in the top left panel of Figures 9 and 10). The two thinner vertical dashed lines (black) are the limits of the SLD region. In these figures, the top and middle panels are the distributions for temperature (left) and salinity (right), whereas the bottom ones are the differences NoAGRS *minus* Control, for the two variables. In both JFM and JAS the differences in temperature are confined predominantly in the thermocline, with only small expressions in the mixed layer near the Gulf of Oman and in the southern limit of the SLD during the JAS season.

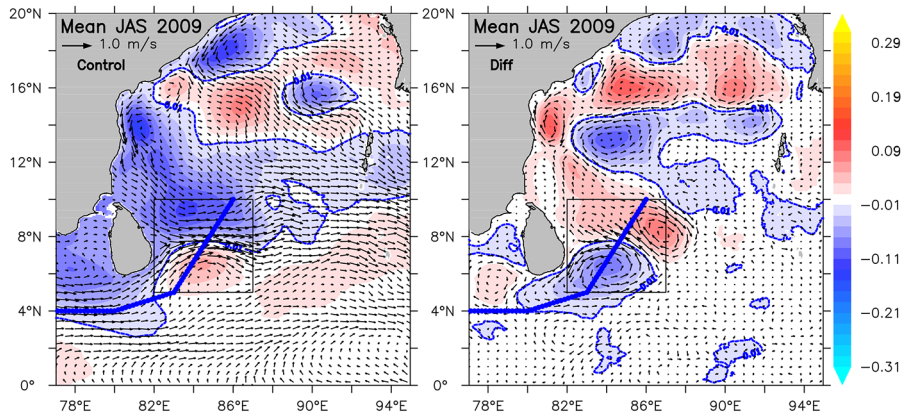


Figure 12. Maps of the seasonal mean (Jun to Sep) of SSH and mixed layer velocity in Control (left) and the difference between NoAGRS and Control (right).

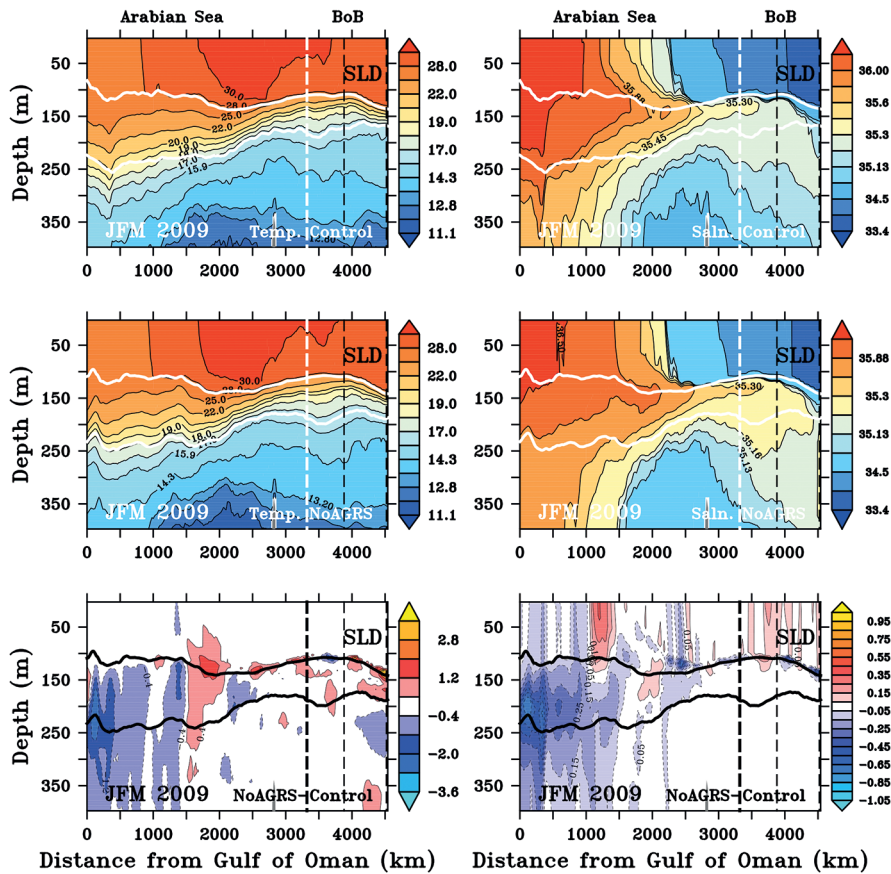


Figure 13. Vertical distributions of salinity and temperature (top two panels) and the differences (NoAGRS minus Control) for JFM.

For salinity, however, the differences are seen in the thermocline and in the mixed layer, in both seasons. Within the SLD region, the anomalies are more expressive in the summer (JAS) season.

In JFM (Figure 13), the mixed layer in the SLD region deepens gradually northeastward, as seen in Figure 9, with no indications of centers of cyclonic or anticyclonic mesoscale features. Very

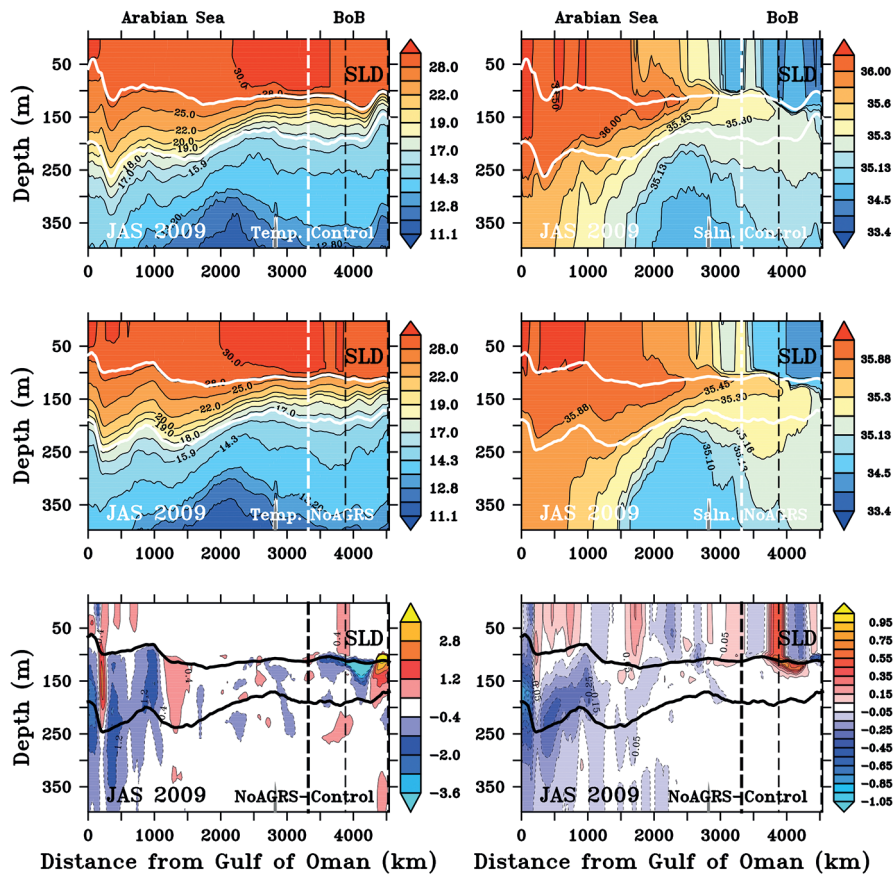


Figure 14. Vertical distributions of salinity and temperature (top two panels) and the differences (NoAGRS minus Control) for JAS. The white curves are the isopycnal surfaces indicating the thermocline region. The thicker dashed line marks the boundary between the ArS and the BoB.

small differences are seen both in temperature and salinity near the isopycnal surface defining the top of the thermocline. In JAS, however (Figure 14), within the SLD region the geometry of the isopycnal indicating the depth of the mixed layer clearly show the presence of an anticyclone (deepening of the mixed layer) in the southern half and a cyclone (shallowing) in the northern part of the SLD, in accordance with what is seen in both Figures 10 and 12. In this season (JAS), the differences in temperature and salinity from two experiments are much more evident, both in the thermocline (mainly for temperature) and in the mixed layer.

As pointed out previously, up to this point, the analyses have focused on the year 2009 because of the more significant differences in the basin averaged KE time series seen in Figure 4. Here, to examine the interannual variability, time series of

the differences averaged over the southern half of the SLD (82°E–87°E, 5°N–7.5°N) are plotted. In the upper, mid, and lower panels of Figure 15 the time evolution of the differences in temperature, salinity, and mixed layer depth between the two experiments are shown, respectively, for the period 2006 to 2013. Despite the negligible mean values, the difference between the variables from the two experiments show significant interannual variability. In the period JAS-2009, the NoAGRS experiment present decrease of approximately 0.2°C and 0.35 in the mixed layer temperature and salinity, respectively, associated with the shallowing of the mixed layer in the order of 15 meters. While the differences in T and S are small in terms absolute, considering larger change in the mixed layer depth represent significant variations in the total heat and salt content.

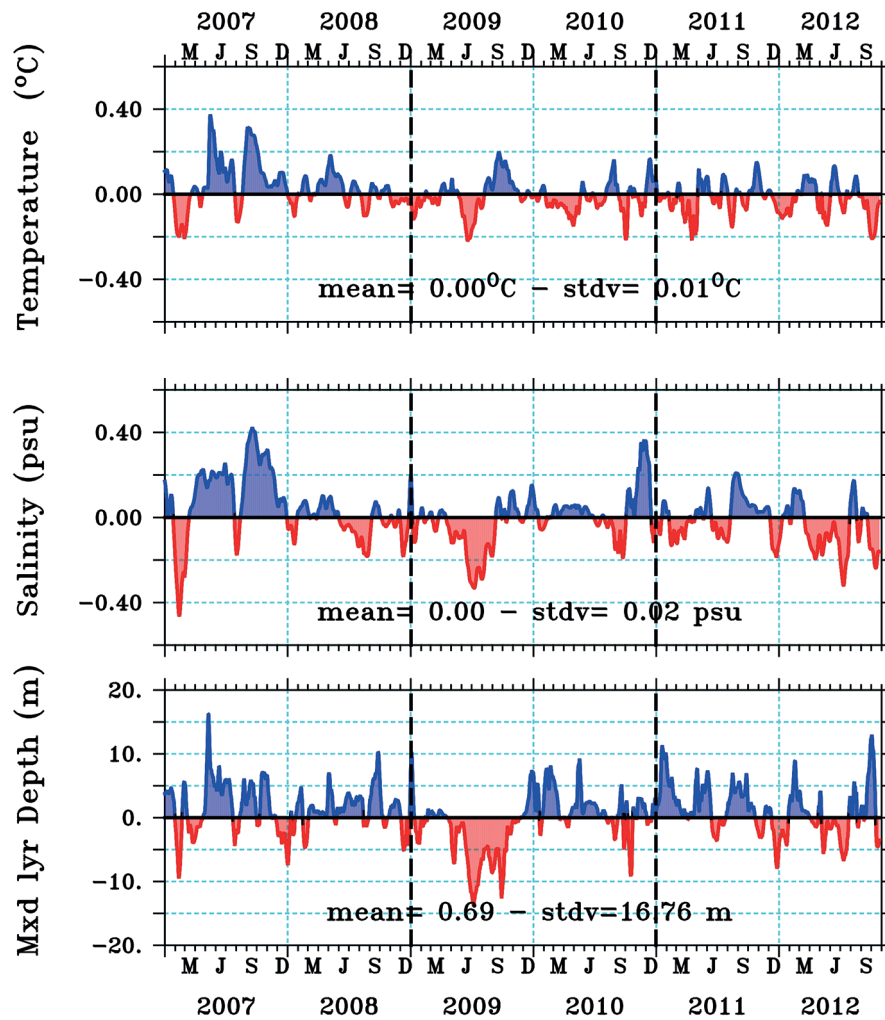


Figure 15. Time series of differences (NoAGRS minus Control) in temperature, salinity and mixed layer depth, averaged over the southern half of the Sri Lanka dome (82°E–87°E, 5°N–7.5°N).

IMPACTS OF AIR-SEA EXCHANGES

Considering the differences in the surface mixed layer resulting from the closure of the PG and RS, it is natural to ask what the impacts on the exchange of thermodynamic variables at the ocean atmosphere interface would be. The HYCOM output at the air-sea interface includes the net evaporation minus precipitation (EMP) and the net total heat flux (QTOT). To evaluate the differences between these fields in the two experiments, the time series of these quantities were averaged over the entire modeled region. Results for the Control experiment and the difference NoAGRS minus control, for JFM and JAS of 2009 are shown in Figure 16. QTOT is in $W m^{-2}$

and EMP in $kg m^{-2}s^{-1}$. Positive values indicate downward fluxes (into the ocean).

The differences between NoAGRS and Control (displayed in the right panels of Figure 16) indicate that the closure of the PG and RS in the numerical simulation results in changes in QTOT of up to $5 W m^{-2}$, mainly in the ArS, during JFM (b). In this season (JFM), changes in EMP (c) with magnitudes of up to $5 kg m^{-2}s^{-1}$ are present, predominantly in the western ArS and in the BoB, with regions with upward and downward fluxes. These regions with variable spatial distribution in the surface fluxes are probably associated with the changes in the upwelling/downwelling regions. In the summer season (JAS), as seen in panels f and h of Figure

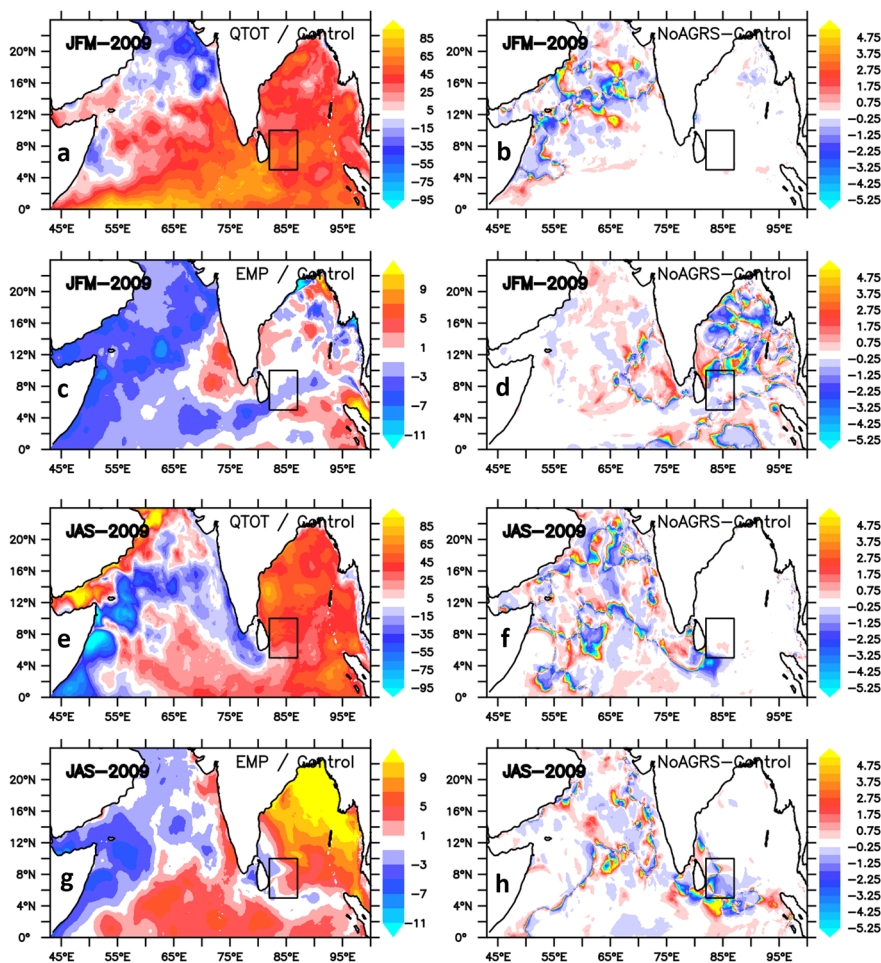


Figure 16. Left panels: Total heat flux (QTOT), in $W m^{-2}$, and excess evaporation (EMP), in $kg m^{-2}s^{-1}$, at the ocean surface for the Control experiment. Right panels: Differences between EMP and QTOT from the two numerical experiments. Both seasons JFM and JAS, are shown.

16, no significant differences between NoAGRS and Control are found in the BoB. However, both QTOT and EMP present high spatial variability in the ArS as well as in the vicinity of Sri Lanka Dome, during JAS.

SUMMARY AND CONCLUSION

Waters from the Red Sea (RSOW) and the Persian Gulf (PGW), despite their relatively small volume fluxes, spread over a large area of the Indian Ocean. The PGW is shallower than the RSOW, spreading in the thermocline and upper levels of the ArS towards the Bay of Bengal. The heavier RSOW, after leaving the Gulf of Aden, is found at depths 600-800m and flows predominantly to the south along the continental slope,

deepening progressively and reaching as far south as the Agulhas Current. However, to what extent they impact the upper ocean stratification and circulation of the northern Indian Ocean it is less clear. This is an important issue in a scenario of global warming and other human-induced changes in those marginal seas. The present work was done as a first step towards a better understanding of the role of those hypersaline waters, with focus on the PGW, as part of investigations being conducted at the American University of Sharjah.

We find that the complete interruption of the PG and RS inflows leads to small but not completely negligible alterations of the stratification and circulation of the northern Indian Ocean. In the numerical experiments, it is found that the difference

between the basin-averaged kinetic energy between the two runs shows interannual variability, reaching up to 10% of the value in the Control experiment, which includes the two marginal seas. The larger differences occur at interannual scales, reflecting an effect of ENSO. Other significant differences are found in the temperature and salinity of the mixed layer and within the thermocline. As expected, the greater impact occur mainly in the ArS but differences in the more remote northern sector of the BoB. The numerical experiments also show significant impact on the air-sea exchanges and in the upper layer's circulation. In particular, the results show that the upwelling system in the Sri Lanka Dome would respond differently to variability of the climate system in the absence of the two marginal seas.

Even though closure of the PG and the RS is not a realistic situation at present, the results of these numerical experiments can be regarded as a contribution to understand the relevance of those waters to the larger scale. If the reduction of the salt influx impacts processes in remote regions, as found in the present work, one can hypothesize that, on the contrary, the increase would also be relevant. To tackle with this question, further experiments are being conducted, in which several other components, such as riverine inflow, increased evaporation and salt content associated with desalination activities are considered.

ACKNOWLEDGMENTS

This work was funded by the American University of Sharjah Faculty Research Grant (FRG) program (Grants FRG19-M-G67 and FRG20-M-S20). The numerical experiments were run at the Oceanographic Institute of the University of São Paulo, in computer resources sponsored by the São Paulo State Foundation for Research Support (FAPESP), through Grants 2011/50552-4 and 2017/09659-6. The output of the simulations used in the analyses is freely available at the SEANOE repository (DOI:10.117882/74139). EJDC acknowledges the Brazilian Council for Scientific and Technological Development (CNPq) for a Research Fellowship (Grant 302503/2019-6).

AUTHOR CONTRIBUTIONS

- E.J.D.C.: Supervision; Conceptualization; Resources; Methodology; Funding Acquisition; Software; Formal Analysis; Investigation; Writing – original draft; Writing – review & editing.
- A.L.G., G.C.: Formal Analysis; Investigation; Writing – review & editing.
- B.K.: Conceptualization; Investigation; Writing – review & editing.
- M.A.: Project Administration; Funding Acquisition; Writing – review & editing.

REFERENCES

- BEAL, L. M., FFIELD, A. & GORDON, A. L. 2000. Spreading of Red Sea overflow waters in the Indian Ocean. *Journal of Geophysical Research: Oceans*, 105(C4), 8549-8564, DOI: <https://doi.org/10.1029/1999jc900306>
- BLECK, R. 2002. An oceanic general circulation model framed in hybrid isopycnic-Cartesian coordinates. *Ocean Modelling*, 4(1), 55-88, DOI: [https://doi.org/10.1016/S1463-5003\(01\)00012-9](https://doi.org/10.1016/S1463-5003(01)00012-9)
- BOWER, A. S., HUNT, H. D. & PRICE, J. F. 2000. Character and dynamics of the Red Sea and Persian Gulf outflows. *Journal of Geophysical Research: Oceans*, 105(C3), 6387-6414, DOI: <https://doi.org/10.1029/1999JC900297>
- BOWER, A. S., JOHNS, W. E., FRATANTONI, D. M. & PETERS, H. 2005. Equilibration and Circulation of Red Sea Outflow Water in the Western Gulf of Aden. *Journal of Physical Oceanography*, 35(11), 1963-1985, DOI: <https://doi.org/10.1175/JPO2787.1>
- BURNS, J. M., SUBRAHMANYAM, B. & MURTY, V. S. N. 2017. On the dynamics of the Sri Lanka Dome in the Bay of Bengal. *Journal of Geophysical Research: Oceans*, 122, 7737-7750, DOI: <https://doi.org/10.1002/2017JC012986>
- CAMPOS, E. 2020. Numerical experiment on the impact of the Persian Gulf and Red Sea on the Northern Indian Ocean. *Seanoë*, DOI: <https://doi.org/10.17882/74139>
- CAMPOS, E. J. D., GORDON, A. L., KJERFVE, B., VIEIRA, F. & CAVALCANTE, G. 2020a. Freshwater budget in the Persian (Arabian) Gulf and exchanges at the Strait of Hormuz. *PLoS One*, 15(5), e0233090, DOI: <https://doi.org/10.1371/journal.pone.0233090>
- CAMPOS, E. J. D., VIEIRA, F., CAVALCANTE, G., KJERFVE, B., ABOULEISH, M., SHAHRIAR, S., MOHAMED, R. & GORDON, A. L. 2020b. Impacts of brine disposal from water desalination plants on the physical environment in the Persian/Arabian Gulf. *Environmental Research Communications*, 2(12), 125003, DOI: <https://doi.org/10.1088/2515-7620/abd0ed>
- CULLEN, K. E. & SHROYER, E. L. 2019. Seasonality and interannual variability of the Sri Lanka dome. *Deep Sea Research Part II: Topical Studies in Oceanography*, 168, 104642, DOI: <https://doi.org/10.1016/j.dsr2.2019.104642>

- DURGADOO, J. V., RÜHS, S., BIASTOCH, A. & BÖNING, C. W. B. 2017. Indian Ocean sources of Agulhas leakage. *Journal of Geophysical Research: Oceans*, 122(4), 3481-3499, DOI: <https://doi.org/10.1002/2016JC012676>
- EZAM, M., GHAZI, E., BIDOKHTI, A. A., AZAD, M. T. & HASSANZADEH, S. 2017. Physical properties of Persian Gulf outflow thermohaline intrusion in the Oman Sea. *Open Journal of Marine Science*, 7, 169,190, DOI: <https://doi.org/10.4236/ojms.2017.71013>
- GORDON, A., SHROYER, E., MAHADEVAN, A., SENGUPTA, D. & FREILICH, M. 2016. Bay of Bengal: 2013 Northeast Monsoon Upper-Ocean Circulation. *Oceanography*, 29(2), 82-91, DOI: <https://doi.org/10.5670/oceanog.2016.41>
- HALLIWELL, G. R. 2004. Evaluation of vertical coordinate and vertical mixing algorithms in the HYbrid-Coordinate Ocean Model (HYCOM). *Ocean Modelling*, 7(3-4), 285-322, DOI: <https://doi.org/10.1016/j.ocemod.2003.10.002>
- HAN, W. & MCCREARY JUNIOR, J. P. 2001. Modeling salinity distributions in the Indian Ocean. *Journal of Geophysical Research: Oceans*, 106(C1), 859-877, DOI: <https://doi.org/10.1029/2000JC000316>
- HORMANN, V., CENTURIONI, L. R. & GORDON, A. L. 2019. Freshwater export pathways from the Bay of Bengal. *Deep Sea Research Part II: Topical Studies in Oceanography*, 168, 104645, DOI: <https://doi.org/10.1016/j.dsr2.2019.104645>
- JOHNS, W. E., YAO, F., OLSON, D. B., JOSEY, S. A., GRIST, J. P. & SMEED, D. A. 2003. Observations of seasonal exchange through the Straits of Hormuz and the inferred heat and freshwater budgets of the Persian Gulf. *Journal of Geophysical Research: Oceans*, 108(C12), 3391, DOI: <https://doi.org/10.1029/2003JC001881>
- KALNAY, E., KANAMITSU, M., KISTLER, R., COLLINS, W., DEAVEN, D., GANDIN, L., IREDELL, M., SAHA, S., WHITE, G., WOOLLEN, J., ZHU, Y., CHELLIAH, M., EBISUZAKI, W., HIGGINS, W., JANOWIAK, J., MO, K. C., ROPELEWSKI, C., WANG, J., LEETMAA, A., REYNOLDS, R., JENNE, R. & JOSEPH, D. 1996. The NCEP/NCAR 40-Year Reanalysis Project. *Bulletin of the American Meteorological Society*, 77(3), 437-472, DOI: [https://doi.org/10.1175/1520-0477\(1996\)077<0437:TNYRP>2.0.CO;2](https://doi.org/10.1175/1520-0477(1996)077<0437:TNYRP>2.0.CO;2)
- MURTY, V. S. N., SARMA, Y. V. B., RAO, D. P. & MURTY, C. S. 1992. Water characteristics, mixing and circulation in the Bay of Bengal during southwest monsoon. *Journal of Marine Research*, 50, 207-228.
- ROCHFORD, D. J. 1964. Salinity maxima in the upper 1000 metres of the North Indian Ocean. *Australian Journal of Marine and Freshwater Research*, 15(1), 1-24, DOI: <https://doi.org/10.1071/mf9640001>
- SCHOTT, F. A., XIE, S. P. & MCCREARY JUNIOR, J. P. 2009. Indian Ocean circulation and climate variability. *Reviews of Geophysics*, 47(1), RG1002, DOI: <https://doi.org/10.1029/2007RG000245>
- SMITH, W. H. F. & SANDWELL, D. T. 1997. Global sea floor topography from satellite altimetry and ship depth soundings. *Science*, 277(5334), 1956-1962, DOI: <https://doi.org/10.1126/science.277.5334.1956>
- VINAYACHANDRAN, P. N., CHAUHAN, P., MOHAN, M. & NAYAK, S. 2004. Biological response of the sea around Sri Lanka to summer monsoon. *Geophysical Research Letters*, 31(1), L01302, DOI: <https://doi.org/10.1029/2003GL018533>
- VINAYACHANDRAN, P. N., SHANKAR, D., VERNEKAR, S., SANDEEP, K. K., AMOL, P., NEEMA, C. P. & CHATTERJEE, A. 2013. A summer monsoon pump to keep the Bay of Bengal salty. *Geophysical Research Letters*, 40(9), 1777-1782, DOI: <https://doi.org/10.1002/grl.50274>
- VINAYACHANDRAN, P., SHARIF, J. & NANJUNDIAH, R. 2015. Impact of river runoff into the ocean on Indian summer monsoon. *Environmental Research Letters*, 10, 054008, DOI: <https://doi.org/10.1088/1748-9326/10/5/054008>
- VOS, A., PATTIARATCHI, C. B. & WIJERATNE, E. M. S. 2014. Surface circulation and upwelling patterns around Sri Lanka. *Biogeosciences*, 11(20), 5909-5930, DOI: <https://doi.org/10.5194/bg-11-5909-2014>
- WYRTKI, K., ROCHFORD, D. J. & BENNETT, E. B. 1971. Oceanographic atlas of the International Indian Ocean Expedition. In: KALUS, W. (ed.). *The international Indian Ocean Expedition, 1959-65*. Washington, DC: U.S. Government Printed Off.
- YOU, Y. & TOMCZAK, M. 1993. Thermocline circulation and ventilation in the Indian Ocean derived from water mass analysis. *Deep Sea Research Part I: Oceanographic Research Papers*, 40(1), 13-56, DOI: [https://doi.org/10.1016/0967-0637\(93\)90052-5](https://doi.org/10.1016/0967-0637(93)90052-5)